

Collisions between discrete surface spatiotemporal solitons in nonlinear waveguide arrays

Dumitru Mihalache and Dumitru Mazilu

Horia Hulubei National Institute for Physics and Nuclear Engineering (IFIN-HH), 407 Atomistilor,
Magurele-Bucharest 077125, Romania

Falk Lederer

Institute of Condensed Matter Theory and Solid State Optics, Friedrich-Schiller Universität Jena, Max-Wien-Platz 1,
D-07743 Jena, Germany

Yuri S. Kivshar

Nonlinear Physics Center, Research School of Physical Sciences and Engineering, Australian National University,
Canberra ACT 0200, Australia

(Received 14 October 2008; published 13 January 2009)

We study the effects associated with spatiotemporal light localization near the edge of a semi-infinite array of weakly coupled nonlinear optical waveguides. It was shown earlier that such a system can support the existence of a novel class of $(2+1)$ -dimensional continuous-discrete spatiotemporal solitons, which are stable in a broad region of their parameters. We analyze the collisions between this type of spatiotemporal optical solitons and demonstrate that such collisions are strongly affected by the presence of the surface. In particular, since these solitons can be located at different distances from the edge of the waveguide array, we observe a variety of collision scenarios and different outcomes. In addition to well-known scenarios of soliton fusion and symmetric scattering, we get strongly asymmetric outcomes that can be understood as soliton switching.

DOI: [10.1103/PhysRevA.79.013811](https://doi.org/10.1103/PhysRevA.79.013811)

PACS number(s): 42.65.Tg, 42.65.Sf, 05.45.Yv

I. INTRODUCTION

The comprehensive theoretical studies performed in the 1980s on the propagation of electromagnetic waves along the boundaries between two continuous dielectric media (where at least one of them is nonlinear) resulted in the unique prediction that optical solitons can be guided by dielectric interfaces when the nonlinear change of the refractive index is of an appropriate sign and of sufficient magnitude to overcome the linear (low power) refractive index difference between the adjacent media [1–8]. It was then shown that the corresponding self-trapped surface states or *surface solitons* would have a power threshold proportional to the linear refractive index difference between the two media and inversely proportional to the strength of the nonlinearity required to compensate for this difference. Because of the huge difficulties in finding suitable dielectric media with large enough optically induced refractive index changes to compensate for the refractive index differences between currently available materials, no successful experiments have been reported to the present date.

However, the interest in the study of nonlinear optical surface waves has been renewed recently, and a series of theoretical predictions [9–18] and subsequent experiments [19–24] demonstrated nonlinearity-induced light localization near the edge of a truncated one-dimensional waveguide array that can lead to the formation of the so-called *discrete surface solitons*. The formation of this soliton can be understood with the help of simple physics [11] as a trapping of a localized surface wave [25] near the repulsive edge of the lattice when the beam power exceeds some threshold value. The specific features of discrete optical surface solitons in several relevant physical settings and other related phenomena that may occur at the surfaces of photonic structures

have been recently reviewed in Refs. [26–28].

The concept of surface solitons has been recently extended to the case of spatiotemporal light localization [29,30] at the edge of semi-infinite waveguide arrays [31,32] or at the surface of two-dimensional photonic lattices [33]. One-parameter families of continuous-discrete spatiotemporal optical solitons in truncated one- and two-dimensional photonic lattices, the so-called *discrete surface spatiotemporal solitons*, were found to exist provided that their power exceeds some threshold values and were found to be stable in certain parts of their existence domains [31,33].

The effect of gain and loss (e.g., due to optical amplifiers and saturable absorbers in such truncated periodic photonic structures) has been also investigated and the corresponding dissipative surface spatiotemporal solitons in one- and two-dimensional photonic lattices were introduced [34,35]. Similar to other types of discrete dissipative solitons in both one- and two-dimensional lattices [36–39], dissipative surface solitons exhibit novel features that, as a result of both discreteness and gain (loss) effects, have no counterpart in either the continuous limit or in other conservative discrete models for both cubic and quadratic nonlinear media [40–45]. Discrete surface spatiotemporal solitons are adequately described by continuous-discrete nonlinear evolution equations similar to those investigated earlier for cubic [46–49] and quadratic [50] nonlinear optical media, which are subject to specific boundary conditions due to the presence of the surface through the lattice truncation.

In this paper, we analyze the outcomes of collisions between continuous-discrete spatiotemporal surface solitons in truncated waveguide arrays. We demonstrate that such collisions are strongly affected by the presence of the waveguide truncation (an effective surface), and in particular, for both collision of solitons initially set at equal distances from the

surface and collision of solitons propagating in two neighboring waveguides, we observe strongly asymmetric outcomes with soliton jumping to the neighboring waveguides that can be understood as novel types of soliton switching via soliton fusion or scattering.

II. DISCRETE SPATIOTEMPORAL SURFACE SOLITONS

We consider an array of weakly coupled nonlinear optical waveguides described, in the tight-binding approximation (or coupled mode theory), by effective discrete nonlinear Schrödinger equations [25]. We take into account the spatiotemporal evolution of light, but also assume that our waveguide array is truncated so that the light localization occurs near its edge [31]. The model investigated in this work is a (2+1)-dimensional one, with two transverse dimensions (the spatial transverse dimension is discrete, while the other transverse dimension is continuous and corresponds to time). The corresponding discrete nonlinear Schrödinger model can be written in the form

$$i\frac{\partial E_1}{\partial z} - \gamma\frac{\partial^2 E_1}{\partial t^2} + E_2 + \sigma|E_1|^2 E_1 = 0,$$

$$i\frac{\partial E_n}{\partial z} - \gamma\frac{\partial^2 E_n}{\partial t^2} + (E_{n+1} + E_{n-1}) + \sigma|E_n|^2 E_n = 0, \quad n \geq 2, \quad (1)$$

where $n=1$ designates the edge of the waveguide array. In this semi-infinite continuous-discrete model (1) the propagation coordinate z and the dispersion coefficient γ are normalized to the intersite coupling V . In deriving Eqs. (1) the actual electric field in the n th guide, \mathbf{E}_n , has been decomposed into the product of the vectorial guided mode profile of the isolated channel waveguide $\mathbf{e}(x, y)$ and the respective mode amplitude \mathcal{E}_n , which can be finally normalized to give $E_n\sqrt{\chi_{\text{eff}}/V\mathcal{E}_n}$, where the effective nonlinear coefficient is $\chi_{\text{eff}} = \frac{\omega}{c} \frac{n_2}{A_{\text{eff}}}$. Here n_2 is the nonlinear refractive index of the material, A_{eff} is the effective mode area, and $\sigma = \pm 1$ defines focusing or defocusing nonlinearity of the waveguide material, respectively.

The one-parameter families of stationary spatiotemporal soliton solutions of the coupled nonlinear Schrödinger equations (1) are looked for as $E_n(t; z) = \exp(i\beta z)E_n(t)$, where the family parameter β is the nonlinearly induced shift of the waveguide propagation constant and the envelope $E_n(t)$ describes the temporal evolution of the solitonlike pulse in the n th waveguide. For the sake of clarity we restrict ourselves here to the case of anomalous dispersion ($\gamma < 0$), self-focusing nonlinearity ($\sigma = +1$) and in-phase solitons. If we scale out the dispersion parameter by the transformation $t \rightarrow \tau\sqrt{|\gamma|}$, we obtain

$$\frac{d^2 E_1}{d\tau^2} - \beta E_1 + E_2 + |E_1|^2 E_1 = 0,$$

$$\frac{d^2 E_n}{d\tau^2} - \beta E_n + (E_{n+1} + E_{n-1}) + |E_n|^2 E_n = 0, \quad n \geq 2. \quad (2)$$

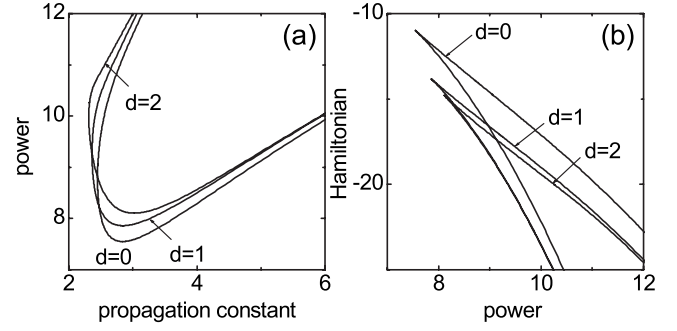


FIG. 1. (a) Normalized power vs propagation constant for the discrete surface light bullets located at distances $d=0$, $d=1$, and $d=2$ from the edge of the array. (b) Hamiltonian vs power for the localized surface modes.

By using a standard band-matrix algorithm [51] to deal with the corresponding two-point boundary-value problem, we found numerically localized solutions $E_n(t)$ of the coupled equations (2) assuming that the amplitude of the pulses in each waveguide, $\max|E_n|$, decays rapidly far from the edge of the waveguide array, so that the corresponding solution describes a mode localized near the surface. The nonlinear modes are characterized by two conserved quantities: the total power P and the system's Hamiltonian H [31]. In Fig. 1 we show both the $P=P(\beta)$ curves of different surface modes located at distances $d=0$, $d=1$, and $d=2$ from the edge of the array and the corresponding $H=H(P)$ dependences. Stable spatiotemporal surface solitons are expected to correspond to positive slopes of the $P=P(\beta)$ curves and to lower branches of the $H=H(P)$ curves; see Figs. 1(a) and 1(b). If we compare the corresponding power curves of different spatiotemporal surface modes, we notice that the threshold power of the mode localized at the edge of the waveguide array ($d=0$) is the lowest one while increasing with the distance d from the surface. Therefore, in sharp contrast to the case of one-dimensional surface solitons [10,11], the surface of a truncated waveguide array creates an effective attractive potential for the spatiotemporal localized modes that reduces the threshold power for mode localization. Figures 2(a)–2(c) show several examples of *stable* nonlinear spatiotemporal continuous-discrete localized states (“discrete surface spatiotemporal solitons”) located at different distances d from the surface for the case of the focusing nonlinearity and for $\beta=4$. The corresponding powers of these stationary solitons are as follows: $P=8.293$ ($d=0$), $P=8.500$ ($d=1$), and $P=8.565$ ($d=2$).

III. OUTCOMES OF THE SOLITON COLLISIONS

Once stable discrete spatiotemporal surface solitons are available, a problem of great interest is to consider collisions between them. In this work, we aim at investigating this issue in the framework of the nonlinear coupled continuous-discrete evolution equations (1), focusing on finding the generic outcomes of collisions between discrete surface spatiotemporal solitons located at different distances d from the edge of the semi-infinite waveguide array. Thus to study generic outcomes of collisions between discrete surface soli-

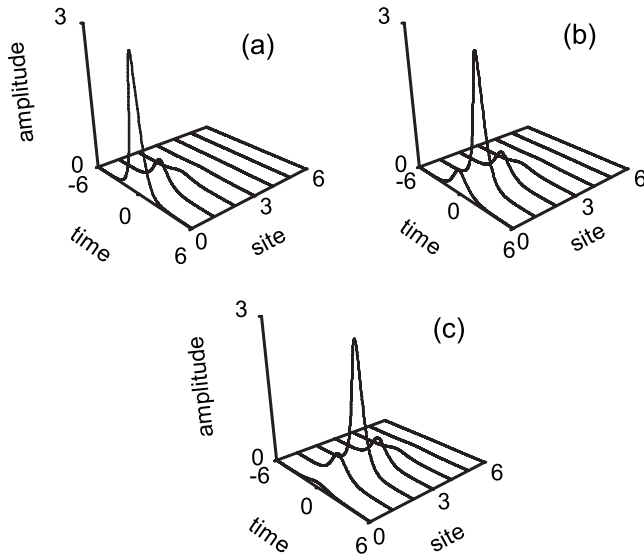


FIG. 2. Examples of *stable* spatiotemporal surface solitons localized at distances of (a) $d=0$, (b) $d=1$, and (c) $d=2$ from the edge of the waveguide array. Here $\beta=4$.

tons, one should take a pair of stable solitons with typical shapes shown in Fig. 2, separated by a large temporal distance $t_2 - t_1 = T$. Thus we solve Eqs. (1) with the initial condition (at $z=0$) corresponding to collisions between two stable surface solitons: $E_n(t,0) = E_n(t+T/2)\exp(i\chi t/2) + E_n(t-T/2)\exp(-i\chi t/2)$, where χ is the kick parameter. Below we take the anomalous group-velocity dispersion $\gamma = -1$ and consider collisions between discrete spatiotemporal solitons located at different distances d from the surface of the semi-infinite waveguide array for various values of the kick pa-

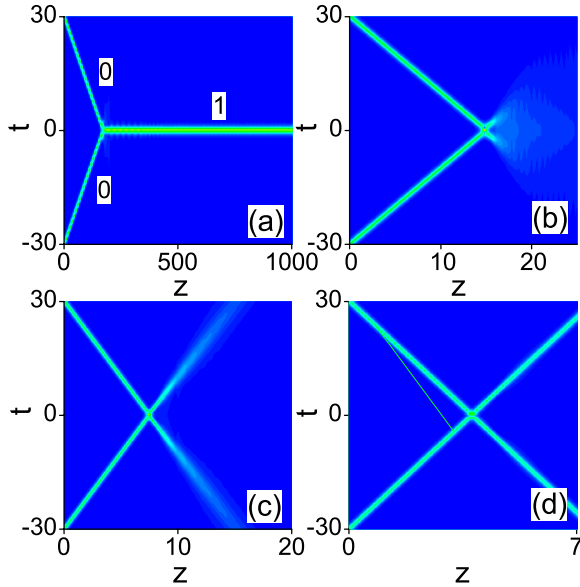


FIG. 3. (Color online) Contour plots display the evolution of the field $|E_n|$ in the plane (t, z) for the collision scenarios of input solitons located at $d=0$, at different values of kick χ : (a) merger into a single soliton located at the distance $d=1$ from the surface, at $\chi=1$, (b) and (c) spreading of the input solitons, at $\chi=2$, and $\chi=4$, respectively, and (d) quasielastic collision, at $\chi=8$. Here $\beta=4$.

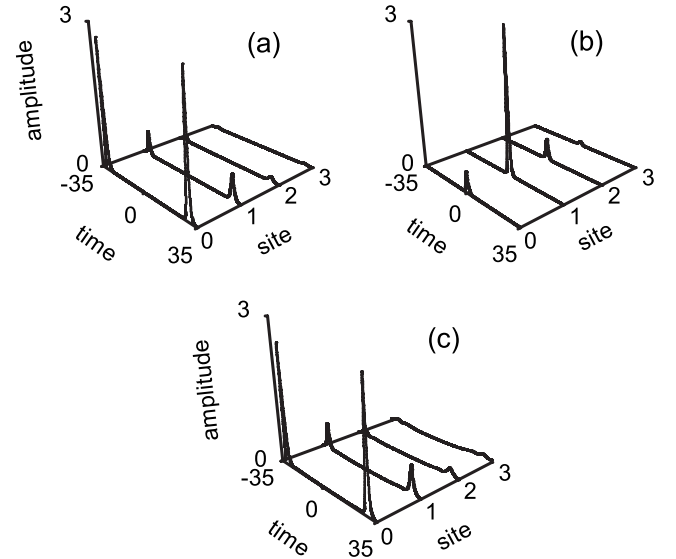


FIG. 4. The field structure at input ($z=0$) (a), at $z=2000$ ($\chi=1$) (b), and at $z=7.5$ ($\chi=8$) (c), corresponding to the two collision scenarios shown in panels (a) and (d) in Fig. 3.

rameter χ and for two representative values of the propagation constant β corresponding to both relatively low and relatively high soliton amplitudes (powers).

We solve the coupled equations (1) with the initial condition (at $z=0$) corresponding to collisions between two stable discrete solitons located either at the same distance $d_1 = d_2 = d$ ($d=0, 1, \dots$) from the surface or at two different distances $d_1 \neq d_2$ from the edge of the semi-infinite array. We employ a Crank-Nicholson finite-difference numerical scheme, with typical transverse and longitudinal step sizes $\Delta t=0.02$ and $\Delta z=0.0005$. The standard transparent boundary

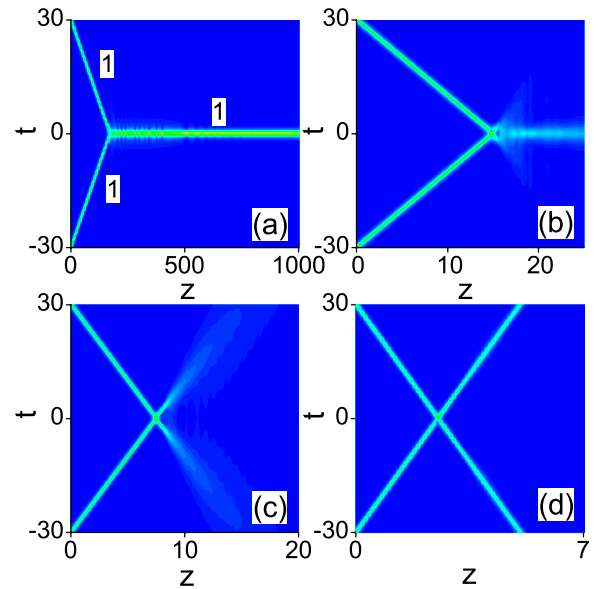


FIG. 5. (Color online) Same as in Fig. 3, but for input solitons located at $d=1$: (a) merger into a single soliton located at the distance $d=1$ from the surface, at $\chi=1$, (b) and (c) spreading of the input solitons, at $\chi=2$, and $\chi=4$, respectively, and (d) quasielastic collision, at $\chi=12$. Here $\beta=4$.

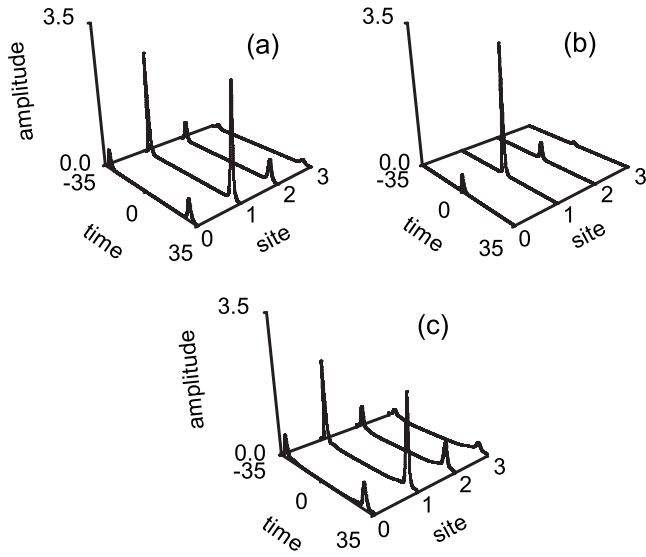


FIG. 6. The field structure at input ($z=0$) (a), at $z=2000$ ($\chi=1$) (b), and at $z=5$ ($\chi=12$) (c), corresponding to the two collisions scenarios shown in panels (a) and (d) in Fig. 5.

conditions [52] were implemented in our numerical code. The resulting nonlinear finite-difference equations were solved using the Picard iteration method [53], and the ensuing linear system was then dealt with using the Gauss-Seidel elimination procedure. To achieve good convergence, five Picard and six Gauss-Seidel iterations were needed. Typically, we used 4001 grid points for the continuous variable t and 31 grid points for the discrete spatial coordinate.

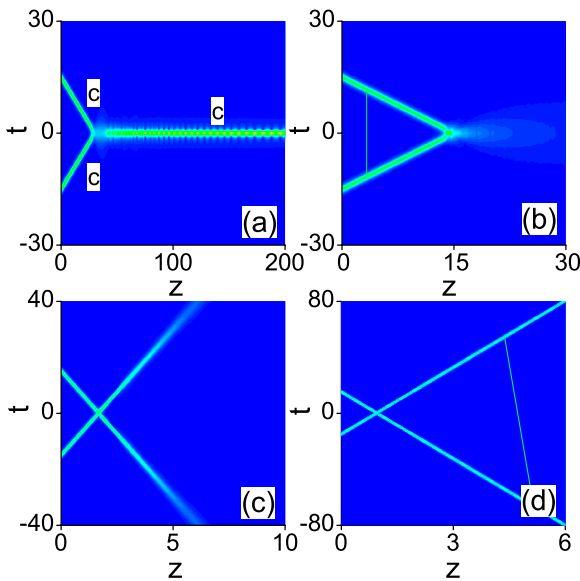


FIG. 7. (Color online) Same as in Fig. 3, but for input solitons located in the center of the lattice: (a) merger into a single soliton located in the center of the lattice, at $\chi=0.5$, (b) and (c) spreading of the input solitons, at $\chi=1$, and $\chi=9$, respectively, and (d) quasielastic collision, at $\chi=16$. Here $\beta=4$.

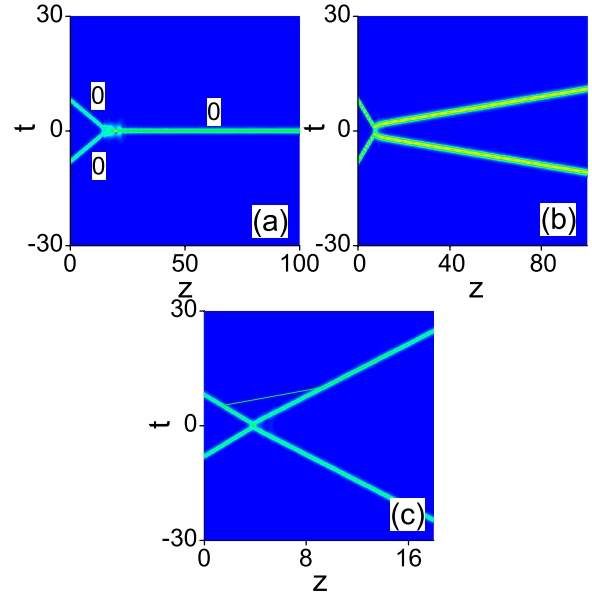


FIG. 8. (Color online) Same as in Fig. 3, but for high amplitude solitons corresponding to $\beta=8$, located at distances $d_1=d_2=0$: (a) $\chi=0.5$, (b) $\chi=1$, and (c) $\chi=2$.

A. Collisions between identical discrete spatiotemporal surface solitons

Next we carry out a series of systematic numerical studies of collisions between two identical discrete spatiotemporal surface solitons initially set at equal distances $d_1=d_2=0, 1, \dots$, from the edge of the truncated waveguide array. First, we consider the collision of solitons of relatively low power (amplitude). In this case, by gradually increasing the initial kick χ , we observe the following three generic outcomes.

(a) *Merger* of two identical solitons into a single soliton at

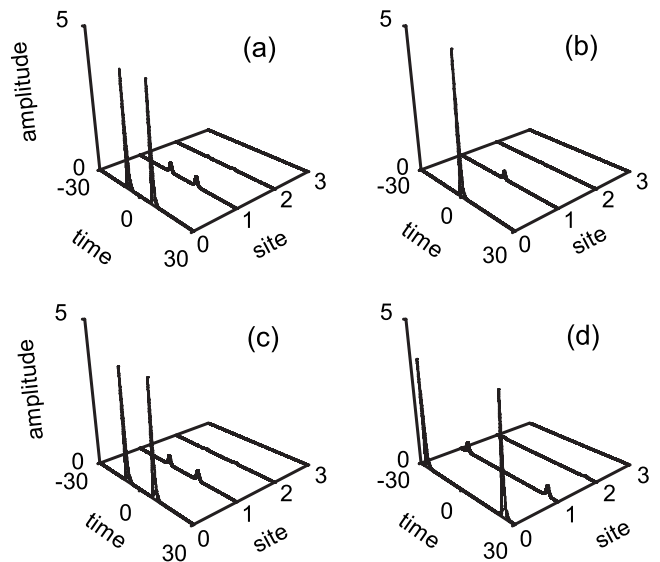


FIG. 9. The field structure at input ($z=0$) (a), at $z=100$ ($\chi=0.5$) (b), at $z=80$ ($\chi=1$) (c), and at $z=18$ ($\chi=2$) (d) corresponding to the collisions scenarios shown in panels (a), (b), and (c) in Fig. 8.

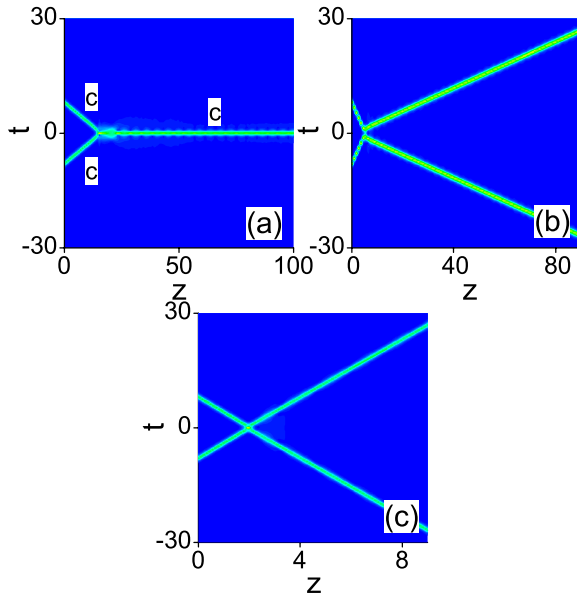


FIG. 10. (Color online) Same as in Fig. 3, but for high amplitude solitons corresponding to $\beta=8$, located in the center of the lattice: (a) $\chi=0.5$, (b) $\chi=1.5$, and (c) $\chi=4$.

relatively small values of the kick parameter χ . The single output soliton may be either located at the same distance from the interface as the input solitons or, more interestingly, it may jump into a neighboring waveguide located at a larger distance from the surface.

(b) *Spreading* of solitons at intermediate values of the kick parameter χ .

(c) *Quasielastic* soliton interactions at large values of χ and the corresponding passage of solitons through each other.

These three distinct collision scenarios are illustrated in Figs. 3–7, showing the field evolution in the plane (t, z) , and by plots of the corresponding field profiles both at input and long after the collision. Surprisingly enough, we find that for the solitons initially set in motion exactly at the edge of the truncated array ($d=0$) the merger process is accompanied by the hopping of the solitons onto the next waveguide situated at a distance $d=1$ from the interface [see Fig. 4(b)], whereas the solitons, which are initially located in the neighboring waveguides (i.e., at distances $d=1$ and $d=2$ from the surface), remain in the same waveguides upon the merging process [see Fig. 6(b) for the case of the solitons located initially at the distance $d=1$ from the lattice edge]. Moreover, for solitons located deep inside the lattice (center solitons c), we get similar collision scenarios as for solitons located near the lattice edge; see Fig. 7.

By increasing the input power (amplitude) of colliding solitons, we observe the disappearance (see Figs. 8–11) of the soliton spreading regime for intermediate values of the kick parameter; in this case, by increasing the collision momentum the solitons gradually “switch” from the merging regime to the quasielastic one [see Figs. 8(b), 8(c), 10(b), and 10(c)]. It is to be mentioned that for both small and intermediate values of the kick parameter, the solitons emerging after collision may have output amplitudes greatly differing

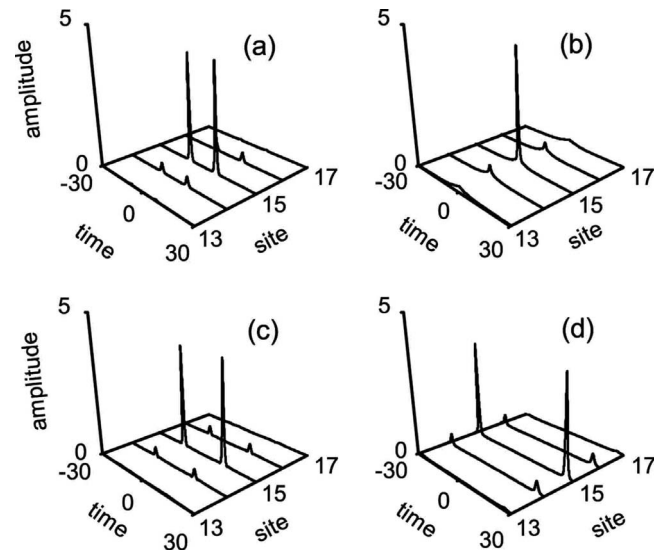


FIG. 11. The field structure at input ($z=0$) (a), at $z=100$ ($\chi=0.5$) (b), at $z=42$ ($\chi=1.5$) (c), and at $z=9$ ($\chi=4$) (d) corresponding to the collisions scenarios shown in panels (a), (b), and (c) in Fig. 10.

from their input ones. Figure 12 shows a typical example when the output amplitude of the soliton can be either larger (in the case of the soliton merging process) [see Fig. 12(a)] or smaller [see Fig. 12(b)] than the input one.

B. Collisions between nonidentical discrete spatiotemporal surface solitons

Next we report results of systematic simulations of collisions between two nonidentical discrete surface spatiotemporal solitons initially set in motion at different distances ($d_1 \neq d_2$) from the edge of the semi-infinite waveguide array. First we consider the case of low amplitude (power) input solitons. Gradually increasing the initial kick χ , we have observed the following three generic collision scenarios.

(a) *Merger* of the two distinct solitons into one of them at relatively small values of the kick parameter χ . This soliton fusion process is accompanied by a drastic change of the velocity of the surviving soliton.

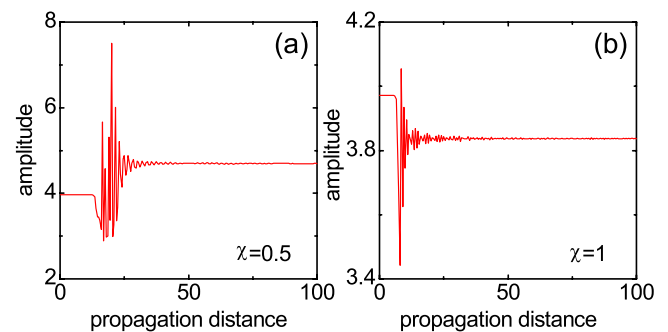


FIG. 12. (Color online) Evolution of the soliton amplitudes corresponding to the collision scenarios shown in Figs. 8(a) and 8(b). Here $\beta=8$, $\chi=0.5$ (a), and $\chi=1$ (b).

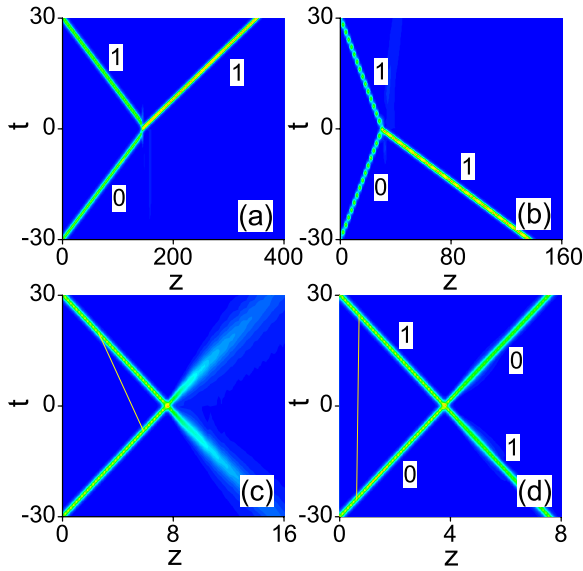


FIG. 13. (Color online) Same as in Fig. 3, but for input solitons located at distances $d=0$ and $d=1$ from the edge of the array. (a) Merger into a single moving “upwards” soliton located at the distance $d=1$ from the surface, at $\chi=0.2$, (b) merger into a single moving “downwards” soliton located at the distance $d=1$ from the surface, at $\chi=1$, (c) spreading of the input solitons, at $\chi=4$, and (d) quasielastic collision, at $\chi=8$.

(b) *Spreading* of solitons at intermediate values of the kick parameter χ .

(c) *Elastic* interactions at large values of χ , and a corresponding passage of solitons through each other.

In Figs. 13(a), 13(b), 14(b), and 14(c) we illustrate a typical soliton fusion scenario in the case of collision of relatively low-amplitude surface solitons located at distances $d_1=0$ and $d_2=1$ from the interface and for relatively small

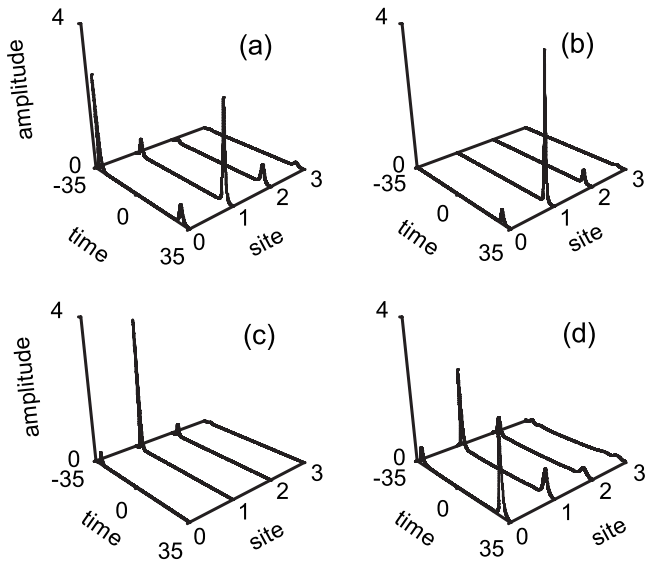


FIG. 14. The field structure at input ($z=0$) (a), at $z=350$ ($\chi=0.2$) (b), at $z=135$ ($\chi=1$) (c), and at $z=7.5$ ($\chi=8$) (d) corresponding to the three collisions scenarios shown in panels (a), (b) and (d) in Fig. 13.

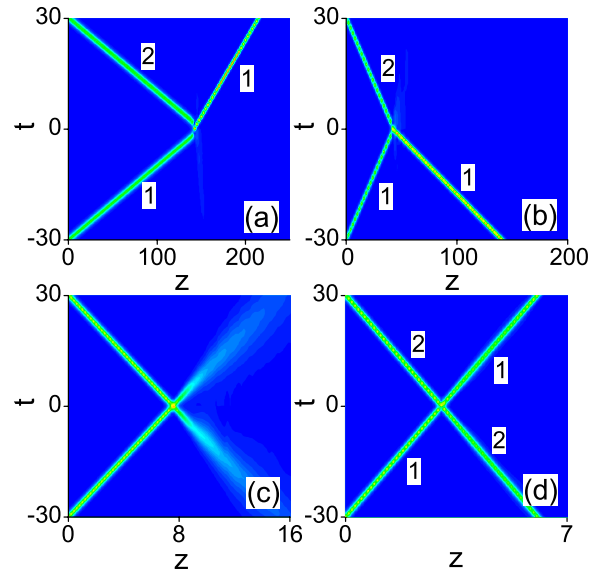


FIG. 15. (Color online) Same as in Fig. 3, but for input solitons located at distances $d=1$ and $d=2$ from the edge of the array. (a) Merger into a single moving “upwards” soliton located at the distance $d=1$ from the surface, at $\chi=0.2$, (b) merger into a single moving “downwards” soliton located at the distance $d=1$ from the surface, at $\chi=0.7$, (c) spreading of the input solitons, at $\chi=4$, and (d) quasielastic collision, at $\chi=10$.

kick parameters χ . Only the soliton located at distance $d_2=1$ survives during this collision process; however, its input velocity is greatly changed after collision [see panels (a) and (b) in Fig. 13]. Similar soliton fusion processes are illustrated in Figs. 15(a), 15(b), 16(b), and 16(c) for the case of collisions between relatively low-amplitude solitons located at distances $d_1=1$ and $d_2=2$ from the interface, when, as before, only the soliton located at distance $d_1=1$ survives.

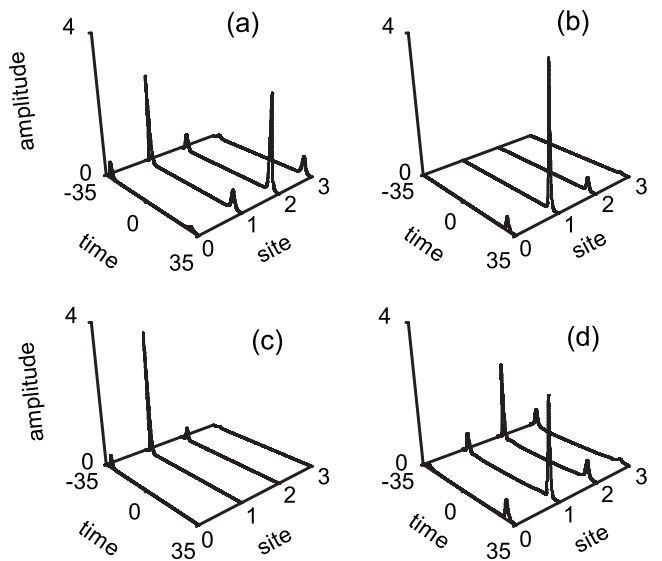


FIG. 16. The field structure at input ($z=0$) (a), at $z=215$ ($\chi=0.2$) (b), at $z=140$ ($\chi=0.7$) (c), and at $z=6$ ($\chi=10$) (d) corresponding to the three collisions scenarios shown in panels (a), (b), and (d) in Fig. 11.

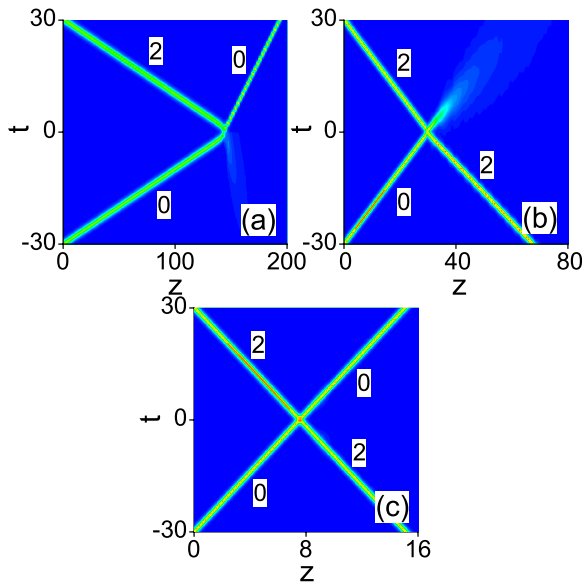


FIG. 17. (Color online) Same as in Fig. 3, but for input solitons located at distances $d=0$ and $d=2$ from the edge of the array. (a) Merger into a single moving “upwards” soliton located at the distance $d=0$ from the surface, at $\chi=0.2$, (b) merger into a single moving “downwards” soliton located at the distance $d=2$ from the surface, at $\chi=1$, and (c) quasielastic collision, at $\chi=4$.

When the input colliding solitons are much more separated spatially—for example, when we consider the input solitons located at distances $d_1=0$ and $d_2=2$ from the interface—the single output soliton resulting from the fusion process may be either one of the two input solitons [see Figs. 17(a) and 17(b) and Figs. 18(b) and 18(c)]. In this case, for relatively low kick parameter χ the output soliton is that centered at the very interface ($d_1=0$) [see Fig. 17(a) and Fig. 18(b)], whereas for a larger value of the kick parameter the output

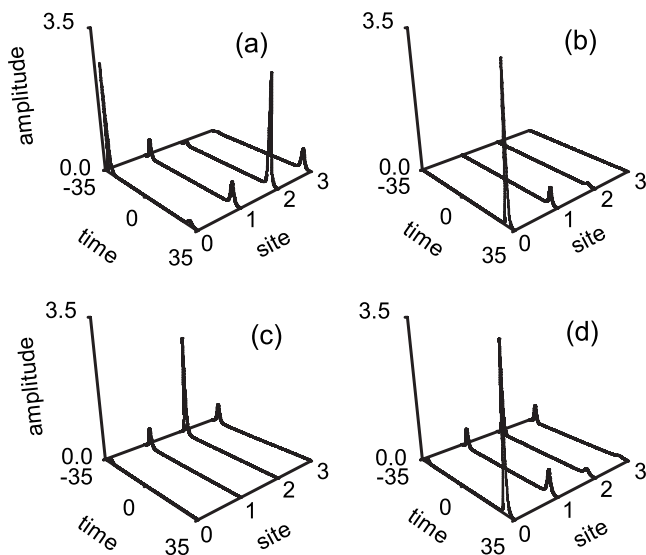


FIG. 18. The field structure at input ($z=0$) (a), at $z=195$ ($\chi=0.2$) (b), at $z=67$ ($\chi=1$) (c), and at $z=15$ ($\chi=4$) (d). The output fields shown in panels (b), (c), and (d) correspond to the three collision scenarios shown in panels (a), (b), and (c) in Fig. 17.

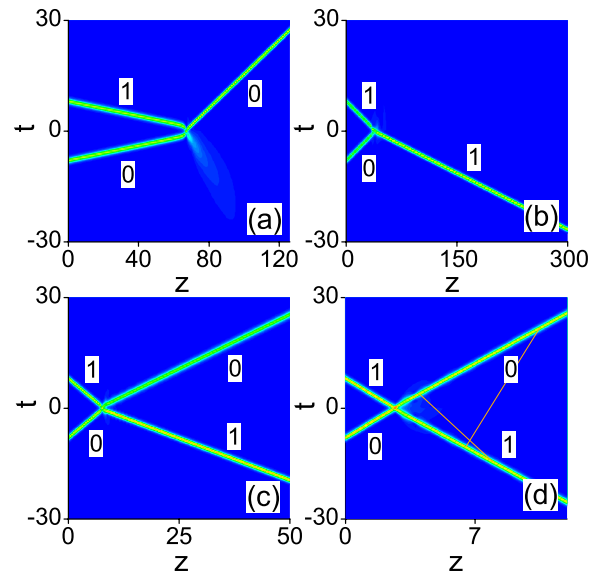


FIG. 19. (Color online) Same as in Fig. 3, but for high-amplitude solitons corresponding to $\beta=8$, located at distances $d_1=0$ and $d_2=1$. (a) $\chi=0.1$, (b) $\chi=0.2$, (c) $\chi=1$, and (d) $\chi=3$.

soliton is that centered at $d_2=2$, deep in the waveguide array. Spreading of the solitons at intermediate values of the kick parameter χ is displayed in Figs. 13(c) and 15(c). By substantially increasing the kick parameter, elastic interactions and a corresponding passage of solitons through each other occur (see Figs. 13–18). As in the case of collision between identical discrete spatiotemporal solitons, by increasing the input power (amplitude) of nonidentical colliding solitons we have observed the disappearance of the spreading soliton regime found for intermediate values of the kick parameter (see Figs. 19 and 20 for a typical example of the collision between solitons located at distances $d_1=0$ and $d_2=1$ from

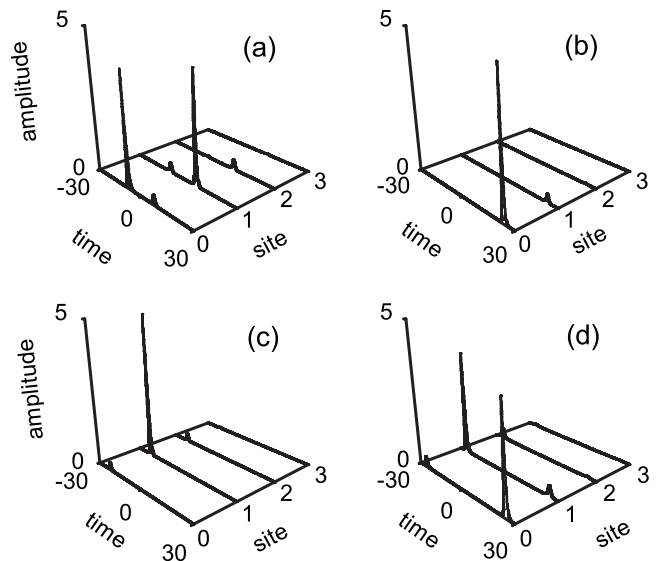


FIG. 20. The field structure at input ($z=0$) (a), at $z=120$ ($\chi=0.1$) (b), at $z=250$ ($\chi=0.2$) (c), and at $z=12$ ($\chi=3$) (d) corresponding to the collisions scenarios shown in panels (a), (b), and (d) in Fig. 19.

the interface). In this case, for relatively low values of the kick parameter only one soliton survives after the collision process; the surviving soliton may be either one of the two input objects [see Figs. 19(a) and 19(b) and Figs. 20(b) and 20(c)].

IV. CONCLUSIONS

We have studied the collision of the continuous-discrete spatiotemporal solitons near the edge of a semi-infinite array of weakly coupled nonlinear optical waveguides. Since these surface spatiotemporal optical solitons can form at different distances from the edge of the waveguide array, we have identified several different collision outcomes and have demonstrated that such collisions are strongly affected by the presence of the surface. We have shown that the outcomes of

the collisions strongly depend on the initial surface soliton parameters, such as the distance of their centers from the surface and their transverse velocities. In particular, in addition to well-known scenarios of soliton fusion and symmetric scattering, we have observed strongly asymmetric collision outcomes. We have pointed out that this novel type of soliton collisions can be understood as a selective soliton switching into the neighboring waveguide via soliton fusion or scattering. We believe that these novel collision scenarios can be found for other types of surface solitons too.

ACKNOWLEDGMENTS

This work was supported in part by the Deutsche Forschungsgemeinschaft (Bonn) in the framework of the Forschergruppe 532 and the Australian Research Council.

-
- [1] W. J. Tomlinson, *Opt. Lett.* **5**, 323 (1980); V. M. Agranovich, V. S. Babichenko, and V. Y. Chernyak, *JETP Lett.* **32**, 512 (1980).
- [2] V. K. Fedyanin and D. Mihalache, *Z. Phys. B: Condens. Matter* **47**, 167 (1982); D. Mihalache, R. G. Nazmitdinov, and V. K. Fedyanin, *Phys. Scr.* **29**, 269 (1984).
- [3] U. Langbein, F. Lederer, and H.-E. Ponath, *Opt. Commun.* **46**, 167 (1983).
- [4] G. I. Stegeman, C. T. Seaton, J. Chilwell, and S. D. Smith, *Appl. Phys. Lett.* **44**, 830 (1984).
- [5] N. N. Akhmediev, V. I. Korneyev, and Y. V. Kuzmenko, *Zh. Eksp. Teor. Fiz.* **88**, 107 (1985) [*Sov. Phys. JETP* **61**, 62 (1985)].
- [6] F. Lederer and D. Mihalache, *Solid State Commun.* **59**, 151 (1986); D. Mihalache, D. Mazilu, and F. Lederer, *Opt. Commun.* **59**, 391 (1986); D. Mihalache, G. I. Stegeman, C. T. Seaton, E. M. Wright, R. Zanoni, A. D. Boardman, and T. Twardowski, *Opt. Lett.* **12**, 187 (1987).
- [7] D. Mihalache, M. Bertolotti, and C. Sibilìa, *Prog. Opt.* **27**, 229 (1989).
- [8] A. D. Boardman, P. Egan, F. Lederer, U. Langbein, and D. Mihalache, in *Nonlinear Surface Electromagnetic Phenomena*, edited by H.-E. Ponath and G. I. Stegeman (Elsevier Science, Amsterdam, 1991), pp. 73–287.
- [9] F. Lederer, L. Leine, R. Muschall, T. Peschel, C. Schmidt-Hattenberger, U. Trutschel, A. D. Boardman, and C. Wächter, *Opt. Commun.* **99**, 95 (1993).
- [10] K. G. Makris, S. Sunstov, D. N. Christodoulides, G. I. Stegeman, and A. Haché, *Opt. Lett.* **30**, 2466 (2005).
- [11] M. I. Molina, R. A. Vicencio, and Yu. S. Kivshar, *Opt. Lett.* **31**, 1693 (2006).
- [12] Y. V. Kartashov, V. A. Vysloukh, D. Mihalache, and L. Torner, *Opt. Lett.* **31**, 2329 (2006); Y. V. Kartashov, L. Torner, and V. A. Vysloukh, *ibid.* **31**, 2595 (2006).
- [13] Y. V. Kartashov, F. Ye, V. A. Vysloukh, and L. Torner, *Opt. Lett.* **32**, 2260 (2007).
- [14] Y. V. Kartashov, V. A. Vysloukh, and L. Torner, *Phys. Rev. A* **76**, 013831 (2007).
- [15] M. I. Molina, Y. V. Kartashov, L. Torner, and Yu. S. Kivshar, *Opt. Lett.* **32**, 2668 (2007).
- [16] Y. Komínis, A. Papadopoulos, and K. Hizanidis, *Opt. Express* **15**, 10041 (2007).
- [17] M. I. Molina, Y. V. Kartashov, L. Torner, and Yu. S. Kivshar, *Phys. Rev. A* **77**, 053813 (2008).
- [18] Z. Xu and Yu. S. Kivshar, *Opt. Lett.* **33**, 2551 (2008).
- [19] S. Sunstov, K. G. Makris, D. N. Christodoulides, G. I. Stegeman, A. Haché, R. Morandotti, H. Yang, G. Salamo, and M. Sorel, *Phys. Rev. Lett.* **96**, 063901 (2006).
- [20] C. R. Rosberg, D. N. Neshev, W. Krolikowski, A. Mitchell, R. A. Vicencio, M. I. Molina, and Yu. S. Kivshar, *Phys. Rev. Lett.* **97**, 083901 (2006).
- [21] E. Smirnov, M. Stepić, C. E. Rütter, D. Kip, and V. Shandarov, *Opt. Lett.* **31**, 2338 (2006).
- [22] B. Alfassi, C. Rotschild, O. Manela, M. Segev, and D. N. Christodoulides, *Phys. Rev. Lett.* **98**, 213901 (2007).
- [23] A. Szameit, Y. V. Kartashov, F. Dreisow, M. Heinrich, T. Pertsch, S. Nolte, A. Tünnermann, V. A. Vysloukh, and L. Torner, *Opt. Lett.* **33**, 1132 (2008).
- [24] X. Wang, A. Samodurov, and Z. Chen, *Opt. Lett.* **33**, 1240 (2008).
- [25] Yu. S. Kivshar and G. P. Agrawal, *Optical Solitons: From Fibers to Photonic Crystals* (Academic Press, San Diego, 2003).
- [26] S. Sunstov, K. G. Makris, G. A. Siviloglou, R. Iwanow, R. Schiek, D. N. Christodoulides, G. I. Stegeman, R. Morandotti, H. Yang, G. Salamo, M. Volatier, V. Aimez, R. Ares, M. Sorel, Y. Min, W. Sohler, X. Wang, A. Bezryadina, and Z. Chen, *J. Nonlinear Opt. Phys. Mater.* **16**, 401 (2007).
- [27] F. Lederer, G. I. Stegeman, D. N. Christodoulides, G. Assanto, M. Segev, and Y. Silberberg, *Phys. Rep.* **463**, 1 (2008).
- [28] Yu. S. Kivshar, *Laser Phys. Lett.* **5**, 703 (2008).
- [29] Y. Silberberg, *Opt. Lett.* **15**, 1282 (1990).
- [30] B. A. Malomed, D. Mihalache, F. Wise, and L. Torner, *J. Opt. B: Quantum Semiclassical Opt.* **7**, R53 (2005).
- [31] D. Mihalache, D. Mazilu, F. Lederer, and Yu. S. Kivshar, *Opt. Express* **15**, 10718 (2007).
- [32] D. Mihalache, D. Mazilu, F. Lederer, and Yu. S. Kivshar, *Opt. Lett.* **32**, 2091 (2007); D. Mihalache, D. Mazilu, Yu. S. Kivshar, and F. Lederer, *Opt. Express* **15**, 10718 (2007).

- [33] D. Mihalache, D. Mazilu, F. Lederer, and Yu. S. Kivshar, *Opt. Lett.* **32**, 3173 (2007).
- [34] D. Mihalache, D. Mazilu, F. Lederer, and Yu. S. Kivshar, *Phys. Rev. A* **77**, 043828 (2008).
- [35] D. Mihalache, D. Mazilu, F. Lederer, and Yu. S. Kivshar, *Phys. Rev. E* **78**, 056602 (2008).
- [36] N. K. Efremidis and D. N. Christodoulides, *Phys. Rev. E* **67**, 026606 (2003).
- [37] E. A. Ultanir, G. I. Stegeman, D. Michaelis, C. H. Lange, and F. Lederer, *Phys. Rev. Lett.* **90**, 253903 (2003).
- [38] U. Peschel, O. Egorov, and F. Lederer, *Opt. Lett.* **29**, 1909 (2004).
- [39] N. K. Efremidis, D. N. Christodoulides, and K. Hizanidis, *Phys. Rev. A* **76**, 043839 (2007).
- [40] Yu. V. Bludov and V. V. Konotop, *Phys. Rev. E* **76**, 046604 (2007).
- [41] N. C. Panoiu, B. A. Malomed, and R. M. Osgood, *Phys. Rev. A* **78**, 013801 (2008); N. C. Panoiu, R. M. Osgood, and B. A. Malomed, *Opt. Lett.* **31**, 1097 (2006).
- [42] Q. E. Hoq, R. Carretero-Gonzalez, P. G. Kevrekidis, B. A. Malomed, D. J. Frantzeskakis, Yu. V. Bludov, and V. V. Konotop, *Phys. Rev. E* **78**, 036605 (2008).
- [43] C. J. Benton, A. V. Gorbach, and D. V. Skryabin, *Phys. Rev. A* **78**, 033818 (2008).
- [44] H. Leblond, B. A. Malomed, and D. Mihalache, *Phys. Rev. A* **77**, 063804 (2008).
- [45] F. Kh. Abdullaev, Yu. V. Bludov, S. V. Dmitriev, P. G. Kevrekidis, and V. V. Konotop, *Phys. Rev. E* **77**, 016604 (2008).
- [46] A. B. Aceves, C. De Angelis, A. M. Rubenchik, and S. K. Turitsyn, *Opt. Lett.* **19**, 329 (1994).
- [47] E. W. Laedke, K. H. Spatschek, and S. K. Turitsyn, *Phys. Rev. Lett.* **73**, 1055 (1994).
- [48] A. B. Aceves, G. G. Luther, C. De Angelis, A. M. Rubenchik, and S. K. Turitsyn, *Phys. Rev. Lett.* **75**, 73 (1995); A. V. Buryak and N. N. Akhmediev, *IEEE J. Quantum Electron.* **31**, 682 (1995).
- [49] A. B. Aceves, M. Santagiustina, and C. De Angelis, *J. Opt. Soc. Am. B* **14**, 1807 (1997).
- [50] Z. Xu, Y. V. Kartashov, L. C. Crasovan, D. Mihalache, and L. Torner, *Phys. Rev. E* **70**, 066618 (2004).
- [51] G. Dahlquist and Å. Björk, *Numerical Methods* (Prentice Hall, Englewood Cliffs, NJ, 1974).
- [52] G. R. Hadley, *Opt. Lett.* **16**, 624 (1991).
- [53] J. M. Ortega and W. C. Rheinboldt, *Iterative Solution of Non-linear Equations in Several Variables* (Academic Press, New York, 1970), p. 182.